Stability of caisson-type breakwater using coupled Fluid-Porous model

Dong Ding[*], Abdellatif Ouahsine[a] and Zhaoyuan Huang[b]

Alliance Sorbonne Université, Université de Technologie de Compiègne,
Laboratoire Roberval Centre de Recherches Royallieu, CS 60319, 60203 Compiegne Cedex, France

Abstract. Breakwaters are used for the protection of harbors and beaches against wave action. This paper focuses on the analysis of the stability of the caisson-type breakwater under Flip-through wave impacts using a coupled Fluid-Porous model. The fluid hydrodynamic is described by the Volume-averaged Reynolds-Averaged Navier-Stokes (VARANS) equation with k-ε model. The flow in the porous medium and armour layer is simulated by the extended Forchheimer law. The developed model is used to estimate the influence of the thickness of armour layer and angle of wave return wall. Thus, a new relation of the overtopping discharge with the thickness of armour layer and angle of wave return wall is established, which can be used to design the structure of breakwater according to the limited value of overtopping wave discharge.

Keywords: caisson-breakwater; waves impacts; CFD simulation; volume-averaged RANS; fluid-porous coupling

1. Introduction

Breakwaters are used to reduce the intensity of offshore wave action, thereby providing safe harbor and shore structures (Sorensen *et al.* 2000). The caisson which uses the mass to resist the overturning force exerted by the waves hitting are usually erected at a place where ships need to be moored or shoreward structures should be protected on the inner face of the breakwater. Furthermore, the armour layer always placed at the toe of the caisson, which typically included shaped concrete armour units or natural rock, is used to resist the wave forces (Kaidi *et al.* 2012, Ding *et al.* 2021).

Wave impacts may ruin the shore structure and cause failures of breakwaters. In front of the vertical walls, wave impacts can cause non-impulsive or impulsive conditions (Bruce *et al.* 2010, Darbani *et al.* 2011). When the waves are relatively small relative to the local water depth and the wave steepness, a non-impulsive situation occurs, where no overtopping waves occur or overtopping waves run up and over the wall giving rise to smoothly-varying loads. In contrast, impulsive conditions occur on vertical walls when waves are relatively higher relative to the local water. Flip-

---

∗Corresponding author, Ph.D., E-mail: dong.ding@utc.fr
[a]Professor, E-mail: ouahsine@utc.fr
[b]Ph.D. Student, E-mail: zhaoyuan.huang@utc.fr

Through Impacts (FTI) are typical impulsive wave impacts. Hattori *et al*. (1994) studied various types of breaking waves and stressed the influence of the Flip-Through Impact (FTI) which may cause the overturning of caissons and rear protective structure. Lugni *et al*. (2006) described three main steps in the flow evolution of FTI: (1) the wave approaching the wall; (2) the wavefront and trough are close to each other, resulting in high vertical flow acceleration; and (3) squeezed wave produces upward-moving jet. The wave overtopping has negative effects on the stability of the harbor or shore structures on the inner slope of the dike and can result in severe damage. The structure of armour layer affects the flow of waves. The armour layers are often built of large armour units and can be considered as a porous medium. Indeed, many recent scientific studies have considered the porosity parameter to represent different types of armour units in the CFD simulations (Van Gent 1996). Traditionally, the Darcy law is used to study linear structures and Forchheimer law is used to investigate non-linear structures for porous medium (Whitaker 1996, Guedda and Ouahsine 2012, Smaoui *et al*. 2008).

In this paper, the stability of breakwater under flip-through impacts (FTI) is presented. The fluid hydrodynamic with the porous medium processes are described by the Volume averaged Reynolds averaged Navier Stokes (VARANS) equation with *k-ε* model in which the flow in the porous medium and armour units is calculated by the extended Forchheimer law. The performance of the stability of caisson-type breakwater is investigated by considering the thickness of armour layer and angle of the wave return wall. Thus, a new relation of the overtopping discharge with the thickness of armour layer and angle of wave return wall is established. The outline of the paper is as follows: in section 2, the governing equations of the fluid and solid coupled model are introduced, the volume-averaged RANS process is detailed. Section 3 is devoted to presenting the configuration of the numerical model and validating the inputting fluid model. Section 4 simulates the solution behavior with various thickness of armour layer and various angles of wave return wall of the caisson. Finally, the conclusions of the study are drawn in section 5.

2. Mathematical formulation for fluid-porous model

In the present work, a free and open-source CFD toolbox OpenFoam is used to investigate the flow around the breakwater. In this section, the mathematical formation of two incompressible phases flow (air and water) in porous medium (armour layer and core), and the process for adjusting to OpenFoam are introduced.

For the turbulence flow, it can be investigated by RANS-VOF equations. The mass and momentum conservation are (Du *et al*. 2018)

$$\nabla \cdot \mathbf{U} = 0 \tag{1}$$

$$\rho \frac{\partial \mathbf{U}}{\partial t} + \rho \nabla \cdot (\mathbf{U}\mathbf{U}) = -\nabla P + \rho \mathbf{g} + \nabla \cdot \left(\mu_{eff} \nabla \mathbf{U}\right) + \sigma \kappa \nabla \alpha \tag{2}$$

while the free surface is tracked by

$$\frac{\partial \alpha}{\partial t} + \nabla \cdot \mathbf{U}\alpha + \nabla \cdot \mathbf{U}_c \alpha (1-\alpha) = 0 \tag{3}$$

where **U** is the velocity vector, **g** denotes the gravitational acceleration vector. *P* is the pseudo-dynamic pressure, *ρ* represents the weighted averaged density, and $\mu_{eff} = \mu + \mu_t$, in which *μ* is the

weighted average dynamic viscosity; and the μ_t is the dynamic turbulence viscosity which is calculated by k-ε model (Shaheed and Gildeh,2009). The surface tension effect is $\sigma\kappa\nabla\alpha$, where $\sigma\mathbf{u}_{water}$ and $\mathbf{u}_{air}$ are the velocity of water and air, respectively, and α is the fluid phase fraction laying between 0 and 1, where $\alpha=0$ corresponds to full of air and $\alpha=1$ corresponds to full of fluid. The last term $\nabla\cdot\mathbf{U}_c\alpha(1-\alpha)$ is an artificial compression term (Higuera *et al.* 2014, Ji *et al.* 2014), where $\mathbf{U}_c=\mathbf{u}_{water}-\mathbf{u}_{air}$.

For the porous medium structures, traditionally, Darcy's law (the first term in Eq. (4) is used to describe flow in the porous medium for linear problems (Hadzalic *et al.* 2018), however, when the non-linear processes take place due to sudden variations in the morphology or of the texture of the bottom, as is the case here, this last law cannot describe the accurately fluid-porous interaction. Then, a correction term (the second term) are added in Eq. (4), based on a quadratic velocity, to take account into this non-linearity. Furthermore, in the present study, an added mass term C_A (Hsu *et al.* 2002) was considered. The reason to consider the added mass is that when a certain amount of water is accelerating, a certain amount of momentum is required. To accelerate the same volume of water in a porous medium, additional momentum is required. It is called added mass because excess extra indicates that a larger volume of fluid must be accelerated (Mendez *et al.* 2001). The extended Forchheimer equation can be written as

$$I = A\mathbf{U} + B\,|\,\mathbf{U}\,|\,\mathbf{U} + C_A\rho\frac{\partial\mathbf{U}}{\partial t} \tag{4}$$

where I is the hydraulic pressure gradient and C_A is an empirical coefficient associated with the added mass.

For the coefficients A and B, several different methods can be used to define (Sidiropoulou *et al.* 2007); here we used the Van Gent's modification Engelund formulas (Van Gent 1996), which can be written as

$$A = \mu_1\frac{(1-\varphi)^3}{\varphi^2}\frac{\mu}{D_{50}^2} \tag{5}$$

$$B = \mu_2(1+\frac{7.5}{K_C})\frac{1-\varphi}{\varphi^2}\frac{\rho}{D_{50}} \tag{6}$$

where D_{50} is the mean diameter of the porous material, φ is the porosity of porous medium, and μ_1 and μ_2 are empirical coefficients related to the linear and nonlinear drag force, respectively. Besides, due to the unsteadiness of the system, the Keulegan-Carpenter number K_C is introduced to describe additional friction (Sarpkaya 1986).

In order to calculate the porous medium flow for RANS equations, the extended Forchheimer equation is added to the Eqs. (1)-(2). However, the extension process is not straightforward, the porosity should be considered; therefore, the hydrodynamic variable $\mathbf{U}$ are be averaged by porosity φ, with respect to the total volume including the fluid volume and the pores. The Volume-Averaged RANS equations (VARANS) can be written as

$$\nabla\cdot\langle\mathbf{U}\rangle = 0 \tag{7}$$

$$(1+C_A)\frac{\rho}{n}\frac{\partial}{\partial t}\langle\mathbf{U}\rangle + \frac{\rho}{n^2}\langle\mathbf{U}\rangle\nabla\langle\mathbf{U}\rangle = -\nabla P + \rho\mathbf{g} + \frac{1}{n}\nabla\cdot\left(\mu_{eff}\nabla\langle\mathbf{U}\rangle\right) + \sigma\kappa\nabla\alpha - A\frac{\langle\mathbf{U}\rangle}{n} - B\,|\,\frac{\langle\mathbf{U}\rangle}{n}\,|\,\frac{\langle\mathbf{U}\rangle}{n} \tag{8}$$

where $\langle \mathbf{U} \rangle$ that exists in the interstices of the solid framework of the porous medium, given by

$$\langle \mathbf{U} \rangle = \frac{1}{V} \int_{V_f} \mathbf{U} dV \tag{9}$$

where $\mathbf{U}$ is the hydrodynamic velocity with respect to the fluid, V is the total volume, and V_f is the part of V which is occupied by the fluid.

The Fluid-Porous model is based on the VARANS-VOF method, which describes the fluid flow with the porous medium processes. The Volume-of-Fluid (VOF) approach is used to describe the volume fraction of each fluid inside each computational cell (Cui *et al*. 2020). The MULES (multidimensional universal limiter for explicit solution) is applied in the OpenFoam, which uses a limiter factor for the flux of the discrete divergence term to make the fluid phase fraction α laying between 0 and 1 (Ouahsine *et al*. 2013). The transport equation can be written as

$$\frac{\partial \alpha}{\partial t} + \frac{1}{n} \nabla \cdot (\alpha \langle \mathbf{U} \rangle) + \frac{1}{n} \nabla \cdot (\alpha(1-\alpha)\langle \mathbf{U_c} \rangle) = 0 \tag{10}$$

In this study, the VARANS equations are numerically implemented in the IHFOAM solver in which the IHMULES are used to account for the porosity. A new algorithm is called PIMPLE, which merged by PISO (pressure implicit with the splitting of operators) and SIMPLE (semi-implicit method for pressure-linked equations) algorithms, are used to obtain the solution of pressure and velocity fields for solving procedure (Higuera *et al*. 2014, Khanh *et al*. 2013, Cai *et al*. 2017).

3. Simulation model and validation

3.1 Simulation model and boundary conditions

Numerical simulations were performed to analyze the flow evolution characterization and forces on the breakwater caissons submitted to FTI (Martin-Medina *et al*. 2018). The numerical breakwater model which is composed of the vertical caisson, porous rubble foundation (core), and seaward armour layer, is shown in Fig. 1.

At the entry of the computational domain, we impose the free surface elevation η deduced from the Airy wave theory (Craik 2004), given by

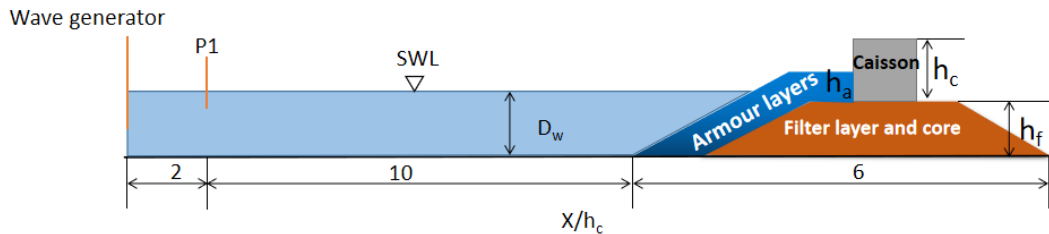$$\eta = \frac{h_w}{2} cos(kx - \omega t + \psi) \tag{11}$$

Fig. 1 Schematic illustration of the numerical model. Caisson height h_c=10 m; Core height h_f=9 m; h_a=2, 4, 6, 8 m is the thickness of armour layer; Wave based on Airy wave theory
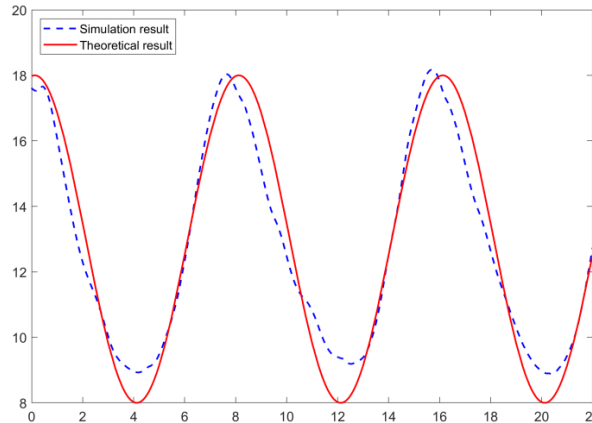
Fig. 2 Comparison between the theoretical results (Eq. (11)) and numerical results

During the simulation, the wave height h_w is set as 10 m, the water depth D_w is set as 13 m. $\omega = \dfrac{2\pi}{T}$, ψ is the wave phase shift and $k = \dfrac{2\pi}{L}$ is the wave number. T=8 s is the wave period and λ=70 m is the wave length.

At the top boundary of the computational domain, we set the atmospheric pressure; while at the bottom boundary we set the slip condition (Ouahsine *et al*. 2013).

3.2 Validation: Response of the waves

The responses of the waves at the neighborhood of the computational domain inlet were investigated and verified. The water height (expressed as $H=\eta+D_w$) between the theoretical results and numerical results at the P1 location are compared and shown in Fig. 2. It shows a good agreement between theoretical and numerical results is met at the neighborhood of the computational domain inlet.

4. Numerical simulation results

4.1 Solution behavior with various thickness of armour layer

The structure of breakwater are shown in Fig. 1. In order to protect the harbor or shoreward, four thickness of armour layer are investigated. Here we assumes h_a/h_c=0.2 is a small armour layer; h_a/h_c=0.4 is a middle armour layer; h_a/h_c=0.6 is a large armour layer, and h_a/h_c=0.8 is a extra-large armour layer for the breakwater.

Fig. 3 shows the shape of the wave according to the armour layer thickness h_a. For breakwaters with porous structures, the increase in the thickness of armour layer will cause a reduction in the transmission coefficient; therefore, less amount of water is hit over the upper part of the caisson; however, the impacting water height becomes large. We note that a larger thickness of armour layer may cause an air pocket between the front of the vertical caisson and waves, and the air may be squeezed and exert a great force on the caisson.
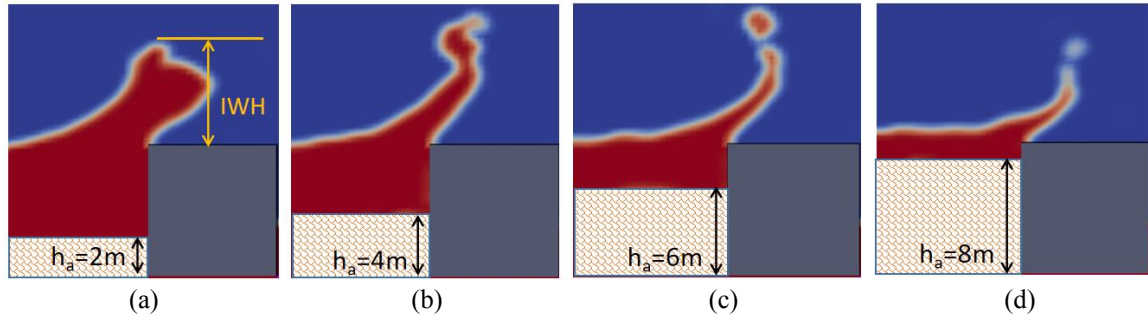
Fig. 3 Wave shape at various thickness of Armour layer (*t*=18.0 *s*): (a) small armour layer h_a/h_c=0.2; (b) middle armour layer h_a/h_c=0.4; (c) large armour layer h_a/h_c=0.6; (d) extra-large armour layer h_a/h_c=0.8
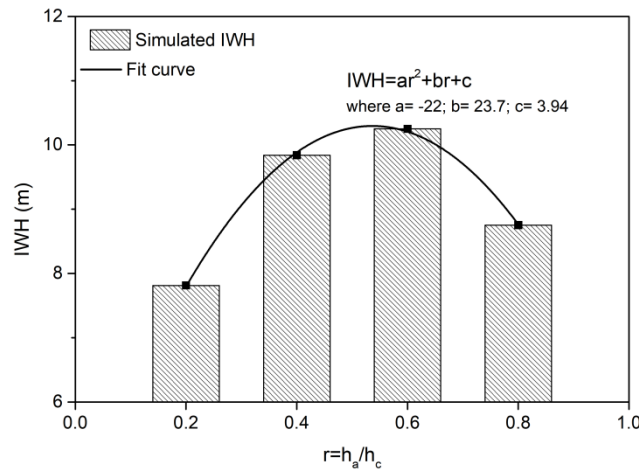

Fig. 4 Impacting wave height and for various thickness of armour layer

We defined the maximum water height along the vertical caisson as the Impacting Wave Height (IWH_{max}) (see Fig. 3). The relationship between the IWH_{max} and the ratio $r=h_a/h_c$ of the armour layer thickness h_a and the caisson height h_c, is given by

$$IWH_{max} = ar^2 + br + c \qquad (12)$$

with a=−22, b=23.7, and the c= 3.94, where the maximum IWH_{max}=10.32 m is obtained for r=0.54 (see Fig. 4).

The overtopping discharge Q is quantified as the water discharge per meter of width W_f that is reaching the shoreward of the caisson, which can be expressed as (Pullen *et al.* 2007)

$$Q = \frac{\iint_S (\mathbf{U} \cdot \mathbf{n}) dS}{W_f} \qquad (13)$$

where **U** is the flow velocity [m/s], **n** represent the normal unit vector. W_f is the width of the fluid flow [m]. S is the surface area of the fluid cross-section at the shoreward of the caisson [m^2].

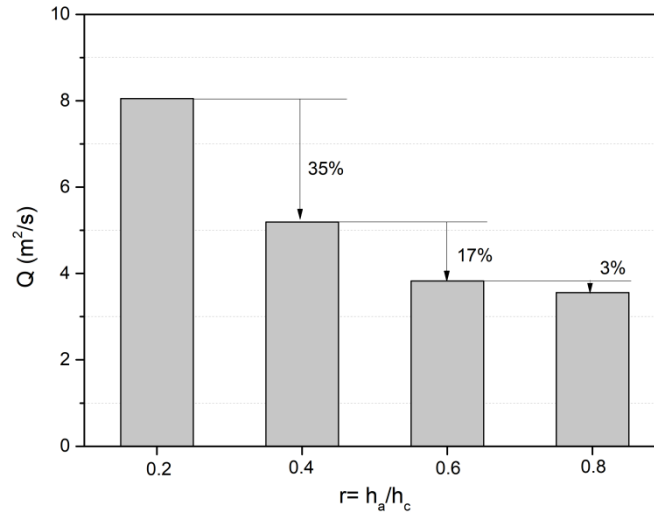The overtopping discharge Q for various thickness of armour layer is shown in Fig. 5. We can

Fig. 5 Mean overtopping discharge rate per metre run of caisson for various thickness of armour layer

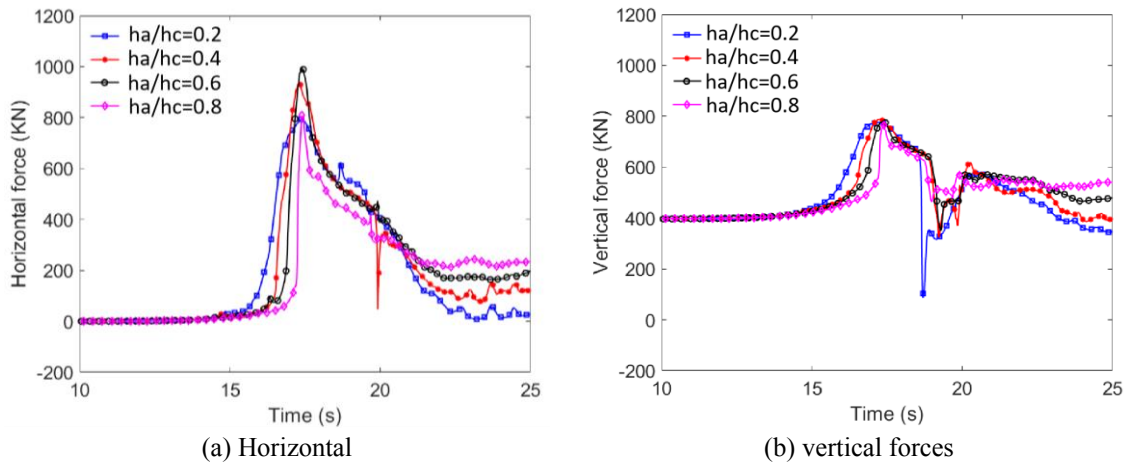(a) Horizontal   (b) vertical forces

Fig. 6 Horizontal and vertical forces for various thickness of armour layer

know that the reduction in the thickness of armour layer clearly contributes to their stability, especially when the thickness ratio is increased from 0.2 to 0.4, the overtopping discharge is reduced by 35%; however, up to the ratio h_a/h_c=0.6, this stability is no longer obvious.

For the motion of caisson, sliding and the overturning always happens because of the Flip-through impacts (Takahashi *et al*. 2014). The forces suffered by the caisson can be obtained by the following equation

$$\mathbf{F}_p = \sum_{i=1}^{N_s} \rho \mathbf{n_i s}_i \qquad (14)$$

where $\mathbf{F}_p$ is the forces contributed from pressure, ρ is the destiny of water, $\mathbf{n}_i$ is normal unit vector, $\mathbf{s}_i$ is the contact face area vector. The horizontal and vertical forces for various thickness of armour
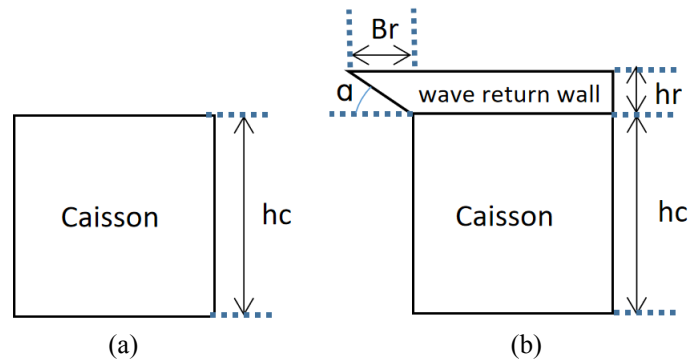
Fig. 7 Shapes of (a) normal caisson and (b) wave return wall breakwater, where h_c=10 m is the height of caisson; B_r=2 m is the horizontal extension of wave return wall; h_r=2 m is the height of wave return wall, and α is the angle of wave return wall
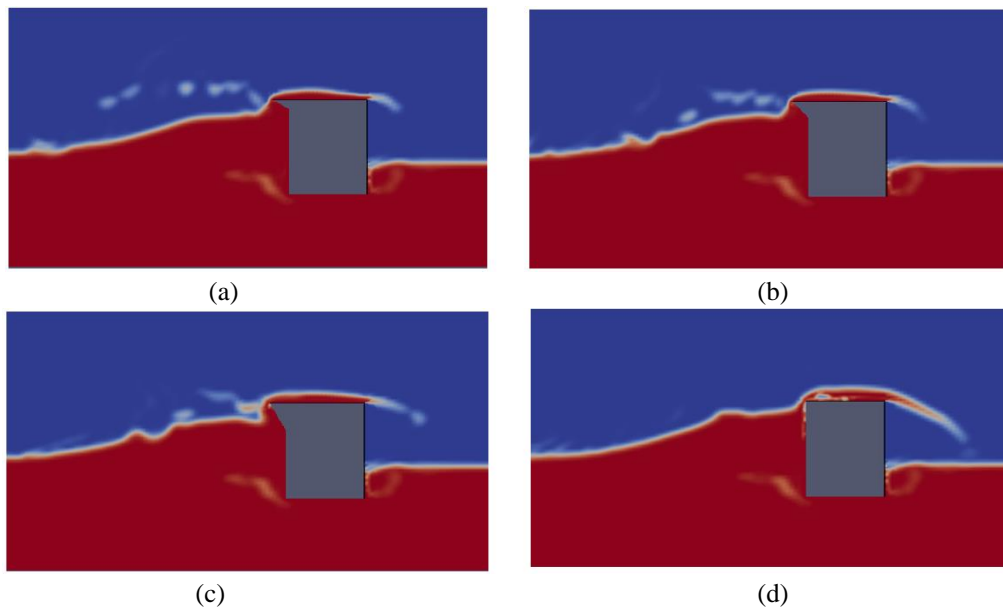

Fig. 8 Waves motion for various angle of wave return wall (h_a=2 m; t=20.0 s): α=(a) 30º; (b) 45º; (c) 60º; (d) 90º

layer are shown in Fig. 6. The peak of the horizontal force happens at about 17.5 s, the peak of the four thickness are 794 KN, 934 KN, 998 KN and 808 KN, therefore, the middle (h_a/h_c=0.4) and large thickness (h_a/h_c=0.6) have larger horizontal forces.

The maximum values of vertical forces have not much difference, however, the higher the thickness, the later the peak of vertical force appears. Therefore, the vertical impact force can be delayed because of the higher thickness.

4.2 Solution behavior with various angles of wave return wall

A new form wave return wall is introduced for the shore protection (Pullen *et al.* 2007), as shown

in Fig. 7. The influence of angle of return wall are investigated, the waves motion for four angles 30°, 45°, 60° and 90° are simulated and shown in Fig. 8. We can conclude that the return wave wall can change the wave shapes significantly, and the overtopping water volume can be drastically reduced.

A dimensionless discharge parameter Q^* were always used to investigate the wave overtopping, which is defined by (Herbert *et al.* 1995, Pullen *et al.* 2007)

$$Q^* = \frac{Q}{\sqrt{gH_{m0}^3}} \tag{15}$$

where g=9.81 m/s^2 is the acceleration due to gravity, H_{m0} is the significant wave height, which is defined as the average wave highest of 1/3 of the waves. We also define the non-dimensionalized the thickness of armour layer: $r=h_a/h_c$ and angle of return wall. Then, we calculate the dimensionless wave overtopping discharge for the dimensionless thickness r and angle q. The results are shown in Table. 1. We can that the smallest wave overtopping discharge occurs when the wave return wall angle α is about 45°.
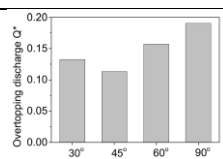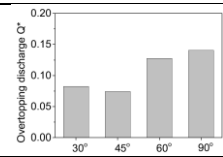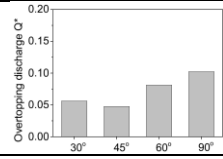
Therefore, the dimensionless wave overtopping discharge Q^* can be fitted in Fig. 9 by the following formula

$$Q^* = \sum_{m+n=0}^{m+n=3} C_{m,n} r^m q^n \qquad m = 0,1,2 \qquad n = 0,1,2,3 \tag{16}$$

where C00=0.106, C10=-0.03043, C01=0.07965, C20=0.002455, C11=-0.001459, C02=0.01456, C21=-0.002049, C12=-0.002502, C03=-0.03519.

Fig. 10 shows the variation of overtopping discharge Q^* for various thicknesses of armour layer and angles of the return wall. According to Eq. (16) and Fig. 10, we can set a limit of overtopping discharge for the breakwater, while considering economic factors to choose the different thicknesses of armour layer and modified caisson. Therefore, this study not only reduces the overtopping

Table 1 Wave overtopping discharge for various thickness of armour layer and angle of return wall

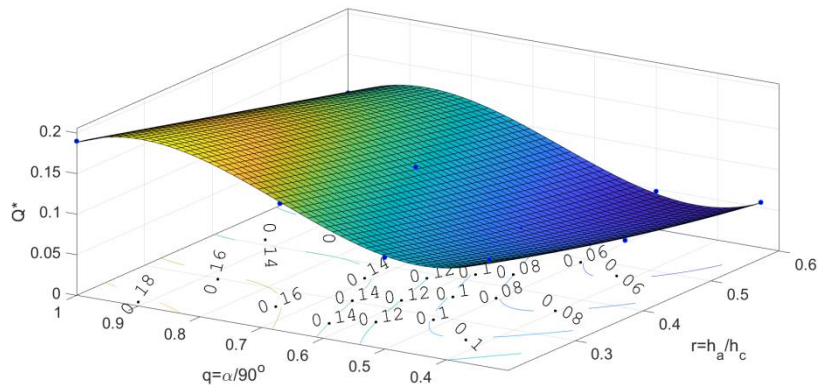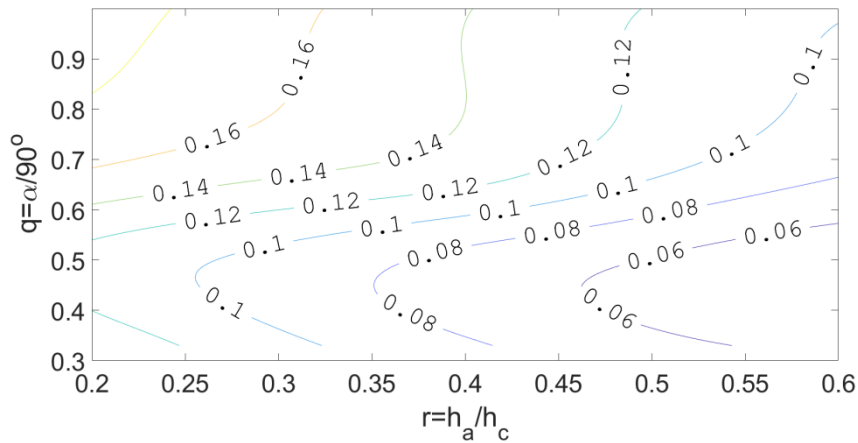| Armour layer thickness $r=h_a/h_c$	Angle of return wall $q=\alpha/90°$	Dimensionless discharge parameter Q^*	Illustration
0.2	0.33	0.133	
	0.50	0.113	
	0.67	0.157	
	1.00	0.190	
0.4	0.33	0.083	
	0.50	0.074	
	0.67	0.128	
	1.00	0.141	
0.6	0.33	0.056	
	0.50	0.047	
	0.67	0.081	
	1.00	0.102	

Fig. 9 Fitted face

Fig. 10 Variation of overtopping discharge Q^* for various thickness of armour layer

discharge according to the specific situation but also considers the economy to choose the structure of armour layer and caisson, which can give a guide to the optimization design.

5. Conclusions

A coupled Fluid-Porous model was proposed to study the stability of the breakwater under hydrodynamic flip-through impacts. The Fluid-Porous model is based on the VARANS-VOF method, which describes the fluid flow with the porous medium processes. The results show that the thickness of armour layer reduces the effects of the breaking waves and that the larger the porous layer is; the less overtopping discharge will be. However, the height of the impact wave reaches the maximum value when the ratio $r=h_a/h_c$ approaches a critical value, which, in the present investigations is equal to $r=0.54$. Furthermore, the smallest wave overtopping discharge occurs when the wave return wall angle is about 45°. Thus, a new relation of the overtopping discharge with the thickness of armour layer and angle of wave return wall was established, which can be used to design the structure of breakwater according to the limited value of overtopping wave discharge.

Acknowledgments

References

Bruce, T., Van Der Meer, J., Pullen, T. and Allsop, W. (2010), "Wave overtopping at vertical and steep structures", Handbook of Coastal and Ocean Engineering, 411-439.

Cai, S.G., Ouahsine, A., Favier, J. and Hoarau, Y. (2017), "Moving immersed boundary method", *Int. J. Numer. Meth. Fluid.*, **85**(5), 288-323. https://doi.org/10.1002/fld.4382.

Craik, A.D. (2004), "The origins of water wave theory", *Ann. Rev. Fluid Mech.*, **36**, 1-28. https://doi.org/10.1146/annurev.fluid.36.050802.122118.

Cui, F., Daskiran, C., King, T., Robinson, B. and Lee, K. (2020), "Modeling oil dispersion under breaking waves. Part I: Wave hydrodynamics", *Environ. Fluid Mech.*, **20**, 15271551. https://doi.org/10.1007/s10652-020-09753-7.

Darbani, M., Ouahsine, A., Villon, P., Naceur, H. and Smaoui, H. (2011), "Meshless method for shallow water equations with free surface flow", *Appl. Math. Comput.*, **217**(11), 5113-5124. https://doi.org/10.1016/j.amc.2010.07.048.

Ding, D., Ouahsine, A., Xiao, W. and Du, P. (2021), "CFD/DEM coupled approach for the stability of caisson-type breakwater subjected to violent wave impact", *Ocean Eng.*, **223**, 108651. https://doi.org/10.1016/j.oceaneng.2021.108651.

Du, P., Ouahsine, A. and Sergent, P. (2018), "Hydrodynamics prediction of a ship in static and dynamic states", *Coupl. Syst. Mech.*, **7**(2), 163-176. http://doi.org/10.12989/csm.2018.7.2.163.

Guedda, M. and Ouahsine, A. (2012), "Similarity solutions of MHD flows in a saturated porous medium", *Eur. J. Mech.-B/Fluid.*, **33**, 87-94. https://doi.org/10.1016/j.euromechflu.2011.12.002.

Hadzalic, E., Ibrahimbegovic, A. and Dolarevic, S. (2018a), "Fluid-structure interaction system predicting both internal pore pressure and outside hydrodynamic pressure", *Coupl. Syst. Mech.*, **7**(6), 649-668. http://doi.org/10.12989/csm.2018.7.6.649.

Hattori, M., Arami, A. and Yui, T. (2011), "Wave impact pressure on vertical walls under breaking waves of various types", *Coast. Eng.*, **22**(1), 79-114. https://doi.org/10.1016/0378-3839(94)90049-3.

Herbert, D.M., Allsop, N.W.H. and Owen, M.W. (1995), "Overtopping of sea walls under random waves", *24th International Conference on Coastal Engineering*, 1130-1142.

Higuera, P., Lara, J.L. and Losada, I.J. (2014), "Three-dimensional interaction of waves and porous coastal structures using OpenFOAM. Part I: Formulation and validation", *Coast. Eng.*, **83**, 243-258. https://doi.org/10.1016/j.coastaleng.2013.08.010.

Hsu, T.J., Sakakiyama, T. and Liu, P.L. (2002), "A numerical model for wave motions and turbulence flows in front of a composite breakwater", *Coast. Eng.*, **46**(1), 25-50. https://doi.org/10.1016/S0378-3839(02)00045-5.

Ji, S., Ouahsine, A., Smaoui, H. and Sergent, P. (2014), "3D Modeling of sediment movement by ships-generated wakes in confined shipping channel", *Int. J. Sedim. Res.*, **29**(1), 49-58. https://doi.org/10.1016/S1001-6279(14)60021-4.

Kaidi, S., Rouainia, M. and Ouahsine, A. (2012), "Stability of breakwaters under hydrodynamic loading using a coupled DDA/FEM approach", *Coast. Eng.*, **55**, 62-70. https://doi.org/10.1016/j.oceaneng.2012.07.035.

Lugni, C., Brocchini, M. and Faltinsen, O.M. (2011), "Wave impact loads: The role of the flip-through", *Phys. Fluid.*, **18**(12), 122101. https://doi.org/10.1063/1.2399077.

Martin-Medina, M., Abadie, S., Mokrani, C. and Morichon, D (2018), "Numerical simulation of flip-through impacts of variable steepness on a vertical breakwater", *Appl. Ocean Res.*, **75**, 117-131. https://doi.org/10.1016/j.apor.2018.03.013.

Mendez, F.J., Losada, I.J. and Losada, M.A. (2001), "Mean magnitudes induced by regular waves inpermeable

submerged breakwaters", *J. Waterw. Port Coast. Ocean Eng.*, **127**(1), 7-15.

Ouahsine, A., Smaoui, H., Meftah, K., Sergent, P. and Sabatier, F. (2013), "Numerical study of coastal sandbar migration, by hydro-morphodynamical coupling", *Environ. Fluid Mech.*, **13**(2), 169-187. https://doi.org/10.1007/s10652-012-9252-5.

Pullen, T., Allsop, N.W.H., Bruce, T., Kortenhaus, A., Schüttrumpf, H. and Van der Meer, J.W. (2007), *EurOtop Wave Overtopping of Sea Defences and Related Structures: Assessment Manual*.

Sarpkaya, T. (1986), "Force on a circular cylinder in viscous oscillatory flow at low Keulegan-Carpenter numbers", *J. Fluid Mech.*, **165**, 61-71.

Shaheed, R., Mohammadian, A. and Gildeh, H.K. (2019), "A comparison of standard k-ε and realizable k-ω turbulence models in curved and confluent channels", *Environ. Fluid Mech.*, **19**(2), 543-568. ttps://doi.org/10.1007/s10652-018-9637-1.

Sidiropoulou, M.G., Moutsopoulos, K.N. and Tsihrintzis, V.A. (2007), "Determination of Forchheimer equation coecients *a* and *b*", *Hydrol. Proc.*, **21**(4), 534-554. https://doi.org/10.1002/hyp.6264.

Smaoui, H., Zouhri, L. and Ouahsine, A. (2008), "Flux-limiting techniques for simulation of pollutant transport in porous media: Application to groundwater management", *Math. Comput. Model.*, **47**(2), 47-59. https://doi.org/10.1016/j.mcm.2007.02.006.

Sorensen, J.D and Burcharth, H.F. (2000), "Reliability analysis of geotechnical failure modes for vertical wall breakwaters", *Comput. Geotech.*, **26**(3), 225{246.

Takahashi, H., Sassa, S., Morikawa, Y., Takano, D. and Maruyama, K. (2014), "Stability of caisson-type breakwater foundation under tsunami-induced seepage", *Soil. Found.*, **54**(4), 789-805. https://doi.org/10.1016/j.sandf.2014.07.002.

Tran Khanh, T., Ouahsine, A., Naceur, H. and ELWassifi, K. (2013), "Assessment of ship manoeuvrability by using a coupling between a nonlinear transient manoeuvring model and mathematical programming techniques", *J. Hydrodyn.*, **25**(5), 788-804. https://doi.org/10.1016/S1001-6058(13)60426-6.

Van Gent, M.R.A. (1996), "Wave interaction with permeable coastal structures", *Int. J. Rock Mech. Min. Sci. Geomech. Abs.*, **6**(33), 277A.

Whitaker, S. (1996), "The Forchheimer equation: a theoretical development", *Tran. Porous Media*, **25**(1), 27-61. https://doi.org/10.1007/BF00141261.